This article has been accepted for publication in a future issue of this journal, but has not been fully edited. Content may change prior to final publication. Citation information: DOI 10.1109/TPEL.2019.2934676, IEEE Transactions on Power Electronics

An SSHI Rectifier for Triboelectric Energy Harvesting

Xian Li, *Student Member, IEEE*, Ye Sun*, *Member, IEEE*

***Abstract*—In this paper, a synchronized switching harvesting on inductor (SSHI) based rectifier for triboelectric energy harvesting is reported for the first time. In recent few years, triboelectric energy harvesters (TEHs), also called triboelectric nanogenerators (TENGs) are emerging and extensively studied, which provide promising solutions for converting mechanical energy to electricity as power resources for electronics. To practically power electronics from TENGs, power management module with high energy efficiency is also essential. The state of the art of power management circuits for triboelectric energy harvesting is mainly focused on increasing dc-dc power efficiency technically. In this paper, we report an SSHI rectifying strategy associated with TEH design and provide a new perspective on designing TEHs or TENGs by considering their capacitance concurrently. A new theoretical model is developed for electricity generation from triboelectric energy harvesting considering the introduced pairing capacitance and the impact force in practical condition. We also demonstrate that ultra-low-cost, easy-fabricated TEHs can also generate a reasonable amount of power. The experimental results show that the proposed SSHI rectifier increases the harvested power by 242.83% when compared to that with a full-wave bridge rectifier for a newly designed low-cost TEH. The proposed SSHI interface provides a promising strategy of rectifier design to enhance ac-dc energy efficiency for triboelectric energy harvesting.**

Index Terms*—Triboelectric energy harvesting, TENG, SSHI, rectifier, power efficiency

I. Introduction

Since firstly introduced in 2012 [1], triboelectric energy harvesters (TEHs), namely triboelectric nanogenerators (TENGs) have been studied extensively in recent years. A great number of promising TENGs have been reported, which have shown great potential for providing sustainable power resources for electronics [2]-[6]. The energy conversion in TENGs is based on the mechanism of triboelectricity or contact electricity by which surface charge is generated from contact and separation or sliding between two materials. The generated charge fluctuates periodically with the input vibration, which thus can convert mechanical energy to electrical energy. Previously we also proved that instead of using nanomaterials and micro/nanoscale fabrication as TENGs, low-cost materials and manufacturing techniques can also achieve reasonable results by triboelectric energy harvesting [4]. Thus, we use TEHs throughout the paper for all types of triboelectric energy harvesting devices. The proposed rectifying strategy in this study is universal for all TEHs.

For power management for TEHs to power electronics, full-wave bridge rectifiers are commonly used for ac-dc conversion in current triboelectric energy harvesting studies [5]-[7]. A wide variety of TENGs have been proposed in the state of the art with innovative design, improved power, and flexible and diverse characteristics for various applications; they often adopted bridge rectifiers to convert ac triboelectric pulses to dc power. Some commercial power management integrated circuits (PMICs) with a full-wave bridge rectifier and a buck converter have also been applied for TENGs [8], [9]. Bridge rectifiers are no doubt a simple and effective way to achieve dc power from TEHs but may have the limitation of low power efficiency for mechanical energy harvesting. To enhance the energy efficiency, a few remarkable studies have recently been reported, in which buck-converters are introduced to increase the dc power after rectifiers. Notably, Xi *et al.* [10] proposed a universal power management strategy using dc buck conversion for TENGs. Bao *et al.* [11] developed a power management circuit consisting of a dc-dc management circuit and a bridge rectifier for ac-dc conversion for TENGs. Cheng *et al.* [12] introduced the optimized inductor-capacitor oscillating into a power management circuit to improve the efficiency for TENGs. Park *et al.* [13] proposed a high-voltage dual-input buck converter with maximum power tracking for TENGs.

Among these studies, the proposed buck-converters generally integrate a switching device and an inductor to lower the energy dissipation from the bridge rectifiers to the load. These designs show universality and high-efficiency in the dc-dc stage for different modes of TEHs [10]-[13]. In addition, there are also some studies that have directly applied to switch in the dc-dc conversion for triboelectric energy harvesting. Qin *et al.* [14] investigated transferring and storing energy from TENGs with unidirectional switches and passive power management circuits. Vasandani *et al.* [15] used a synchronous switch to enhance the output performance of TENGs. The switches are equipped into the power management circuit with a bridge rectifier to prevent the charge leakage. For interfacing with harvesters, however, few rectifier designs have been identified so far to enhance power efficiency other than adopting bridge rectifiers.

In this study, we develop a new rectifier for TEHs based on synchronized switching harvesting on inductor (SSHI) technique. SSHI rectifiers have been studied for piezoelectric energy harvesting and can enhance its harvested power and energy efficiency compared to bridge rectifiers [16]-[18]. The SSHI interfaces introduce an optimal switching and an inductor to reduce the energy dissipation and ensure the energy flowing from the mechanical part to the electrical

This work was supported by the National Science Foundation (Award No. 1710862 and 1751454).

X. Li is with the Department of Mechanical Engineering-Engineering Mechanics, Y. Sun is with the Department of Mechanical Engineering-Engineering Mechanics and the Department of Biomedical Engineering, Michigan Technological University, Houghton, MI 49931 USA. (Email: xian@mtu.edu; yes@mtu.edu *Corresponding author.).

This article has been accepted for publication in a future issue of this journal, but has not been fully edited. Content may change prior to final publication. Citation information: DOI 10.1109/TPEL.2019.2934676, IEEE Transactions on Power Electronics

circuit. However, the highly changeable inner capacitance of TEHs leads to difficulty of achieving optimal synchronized switching time for the LC loop composed of the added inductor and the inner capacitance of the TEH, which is one of the keys for successful SSHI rectifier design.

In this paper, we propose an SSHI rectifying strategy for triboelectric energy harvesting and provide a new perspective of designing TEHs with the consideration of their inner capacitance concurrently. To the best of our knowledge, the proposed SSHI rectifier associated with the TEH design in this paper is among the first that provides a new ac-dc design for TEHs and considers the capacitance in TEH design as well. We also develop a theoretical model considering the source capacitance and the impact force to better understand the energy conversion in practical conditions and guide the TEH design. The input motion can be low frequency (less than 10 Hz) and thus can be used for scavenging energy from human motion.

This paper is organized as follows: Section II introduces the design of the new TEH design and the associated new model for triboelectric energy harvesting. Based on the understanding, Section III describes our proposed SSHI rectifier for TEHs. Section IV is the validation experiments and results. Finally, Section V concludes the paper.

II. Triboelectric Energy Harvesters

A. Basis of Triboelectric Energy Harvesters

Contact and separation or sliding between two materials generates charges on each surface, which is so-called triboelectricity or contact electricity. For triboelectric charge generation, material and contact have been identified as the two major contributing factors. Using triboelectricity for energy harvesting is emerging with a great number of TEHs, mainly TENGs, proposed recently. Significant efforts have been put on enhancing material and contact of TENGs for improving power generation and efficiency.

A typical TEH or TENG consists of three major components: two triboelectric material layers for charge generation, two electrode layers, and a substrate for motion conversion. Most materials can act as triboelectric materials as the triboelectric series [19]. Sometimes, for a simplified TEH, one conductive material can be used as both triboelectric material and electrode. In the working process of TENGs, the periodic relative motion between the two triboelectric material layers results in the generation and distribution of electrical charges. The two common modes of triboelectric energy harvesting are related to the two different motions: contact-separation and sliding [20], [21]. We focus on the contact-separation mode in this study.

The energy conversion of a TEH or TENG is based on the charge generation and redistribution resulted from triboelectricity and the changeable distance between two triboelectric material layers. The mechanism of the contact-separation mode for a TEH with one conductive material layer used for both charge generation and one electrode is illustrated in Fig. 1. In this TEH, low-cost materials, foam, and e-textile are used as the triboelectric material layer. The two electrodes are copper and e-textile. The detailed design is described in Section II.B. Fig. 1 (a) is the original state with no charge generated. When contacted, the generated charge distributes

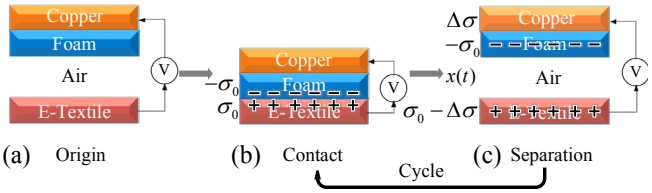

Fig. 1. The mechanism of contact-separation mode of triboelectric energy harvesting: (a) Original state, (b) contact, and (c) separation.

on the contacting surfaces, causing the equal and opposite charge density σ_0 on either contacting surface as shown in Fig. 1 (b). When the contact force is lessened, the separation distance between the two triboelectric material layers increases as shown in Fig. 1 (c), in which an amount of charge is transferred between electrodes and can be collected. Due to the charge redistribution, a potential difference is induced between the two electrodes and changes with the separation distance. The contact-separation process cycles with the periodic input motion and thus converts mechanical motion into electricity.

B. Proposed Multilayer Triboelectric Energy Harvester

Using different triboelectric materials generates a different amount of triboelectric charge basically following the triboelectric series. In our previous experiment [4], foam shows the high capability of charge generation and linear relationship with external work. The results showed that the surface voltage on the foam layer significantly increases linearly with sliding times as shown in Fig. 2. It is also ultra-low cost, highly accessible, flexible, and safe for various applications. E-textile is a wearable conductive material and often used for developing wearable sensors and systems. In this study, we also choose foam and e-textile as triboelectric materials. It shows that low-cost materials and easy-assembly can also achieve reasonable results for triboelectric energy harvesting.

Besides the material, contact is also a critical factor for the charge generation. A multilayer-structure can significantly improve the contact area with the same overall size. It can also ensure a controllable capacitance of the TEHs which is a key to the SSHI design. Thus, we use the multilayer-structure to achieve a pairing capacitor in our TEH design. The design and analysis are illustrated in details as follows.

The proposed TEH with a multilayer-structure design is shown in Fig. 3. On the left side, a basic structure is to keep the contact separation process, while a pairing capacitor with a multilayer structure is shown on the right in Fig. 3. The

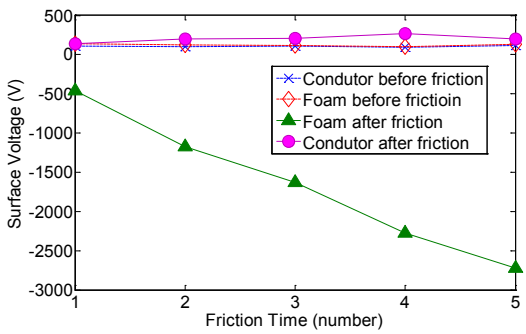

Fig. 2. Triboelectric property of foam [4].

This article has been accepted for publication in a future issue of this journal, but has not been fully edited. Content may change prior to final publication. Citation information: DOI 10.1109/TPEL.2019.2934676, IEEE Transactions on Power Electronics

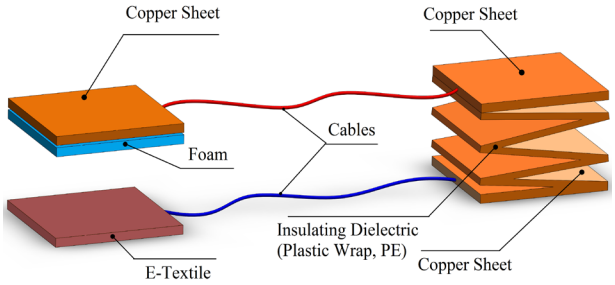

Fig. 3. The structure of the proposed triboelectric energy harvester.

pairing capacitor is multi-folded to a sandwich-like three-layer plate that consists of two copper sheets as the outer layers and a thin polyethylene (PE) layer in between. The PE layer is used as the insulating dielectric and has an approximate thickness of 12.5 μm, which is proper for designing a pairing capacitor with a relatively large capacitance.

The multilayer pairing capacitor is controllable and will stabilize the source capacitance for further SSHI design. The original TEH without the pairing capacitor has a changeable capacitance C_{tribo} which is the series capacitance of the air layer and the foam layer, $\frac{1}{C_{tribo}}=\frac{x(t)}{\varepsilon_0 A}+\frac{1}{C_{Foam}}$, where $x(t)$ is the separation distance between the triboelectric material layers, A is the effective contact area, ε_0 is the permittivity of air, and C_{Foam} is the capacitance of the foam layer. This capacitance, C_{tribo}, is actually highly variable due to the relatively wide range of separation distance, $x(t)$, varying in a range from 100 μm to 10 mm in this case. The capacitance C_{Foam} also changes with its thickness in the mechanical process. The highly changeable source capacitance C_{tribo} brings difficulties to designing an SSHI rectifier interfacing with TEHs as the source capacitance of harvesters is critical for designing the synchronized switching.

When parallel with the pairing capacitor, C_{pair}, which has a relatively large capacitance resulted from the multilayer structure, the inner capacitance of the harvester can be stabilized in a controllable range. In this study, the total capacitance of the proposed TEH, C_T, can be calculated by $C_T = C_{tribo} + C_{pair}$. Here, C_{tribo} represents the capacitance of the basic TEH structure for the distinguishable purpose. By adding the pairing capacitance, the total capacitance of the TEH can only vary by up to 30.03%, which stabilized the C_T for the rectifier design. This multilayer TEH will be then used in our proposed SSHI design.

C. New Model for Triboelectric Energy Harvesting

To further understand triboelectric energy harvesting and guide rectifier design interfacing with TEHs, we first develop a new model considering the source capacitance and the impact force in dynamic process. Some remarkable studies are already carried out to investigate the theoretical model of triboelectric energy harvesting [23], [24]. In practical applications of TENGs, the dynamic mechanical input often generates periodic contact and separation or sliding and therefore generates charges for powering electronics. In the dynamic process of contact and separation, there is an obvious impact force between the two parts of TENGs in most cases due to the fast contact and separation process. However, this impact force is seldom considered in existing models. In this section, the new theoretical model for triboelectric energy harvesting is shown in details.

In existing models, a well-accepted theoretical voltage-charge-distance (V-Q-x) relationship [24] has been given in (1) to model the TENG voltage in the contact-separation mode of triboelectric energy harvesting, which also aligns with our previous equivalent circuit model [25],

$$V=-\frac{Q}{A\varepsilon_0}\left(\frac{d_{Foam}}{\varepsilon_{Foam}}+x(t)\right)+\frac{\sigma x(t)}{\varepsilon_0} \tag{1}$$

where V is the generated voltage across TEHs, Q is the amount of transferred charge between the two electrodes, d_{Foam} and ε_{Foam} represent the thickness and relative dielectric constant of the foam layer, σ is the generated surface charge density, and thus $Q_0=\sigma A$ is the generated amount of charge.

For triboelectric energy harvesting, the contact force has been proved as a critical factor that affects charge generation. Equation (2) shows the relationship between the triboelectric charge and contact force [23]:

$$\sigma A=\left(\frac{F}{E'}\sqrt{\frac{\pi}{m_2}}\right)\frac{\varphi_{Foam}\varepsilon_0}{3ex(t)} \tag{2}$$

where F is the contact force, E' is the equivalent elastic modulus, m_2 is the Root Mean Square (RMS) slope which is a statistical surface parameter and is a constant for a given triboelectric material, φ_{Foam} is the effective or surface work functions of the foam layer, e is the elementary charge which equals to the electric charge carried by a single proton. This equation reveals that the triboelectric charge generation is proportionally affected by the applied contact force.

During continuous dynamic contact and separation cycles in most practical conditions, the contact force in each period is not static due to the fast contact. It is actually an impact force in each contact cycle caused by the dynamic process. This impact force can be calculated by equivalent static force which is the static force multiplied by the actual impact factor as shown in (3):

$$F_e=F\left(1+\sqrt{1+\frac{\dot{x}(t)^2}{g\delta_{st}}}\right) \tag{3}$$

where δ_{st} is the static deflection, $\dot{x}(t)$ is the velocity, F is the contact force in static condition whereas $\left(1+\sqrt{1+\frac{\dot{x}(t)^2}{g\delta_{st}}}\right)$ is the impact factor.

Combining (1)-(3), we can obtain the nonlinear relationship of the voltage with the separation distance and the impact force as represented in (4). In the real harvesting system, there is always a load resistance R_L, and $V=IR_L$, where $I=dQ/dt$ is the current through the load resistance caused by the transferred charge. Thus, we can derive (5) from (4).

This article has been accepted for publication in a future issue of this journal, but has not been fully edited. Content may change prior to final publication. Citation information: DOI 10.1109/TPEL.2019.2934676, IEEE Transactions on Power Electronics

$$V = -\frac{Q}{A\varepsilon_0}\left(\frac{d_{Foam}}{\varepsilon_{Foam}} + x(t)\right) + \frac{F\varphi_{Foam}}{3eAE'}\sqrt{\frac{\pi}{m_2}}\left(1+\sqrt{1+\frac{\dot{x}(t)^2}{g\delta_{st}}}\right) \quad (4)$$

$$R_L\frac{dQ}{dt} = -\frac{Q}{A\varepsilon_0}\left(\frac{d_{Foam}}{\varepsilon_{Foam}} + x(t)\right) + \frac{F\varphi_{Foam}}{3eAE'}\sqrt{\frac{\pi}{m_2}}\left(1+\sqrt{1+\frac{\dot{x}(t)^2}{g\delta_{st}}}\right) \quad (5)$$

By solving (5), the voltage through TEHs, V, has the analytical solution as (6).

$$V(t) = -\frac{F\varphi_{Foam}}{3eAE'}\sqrt{\frac{\pi}{m_2}}\left(1+\sqrt{1+\frac{\dot{x}(t)^2}{g\delta_{st}}}\right) - \frac{\frac{d_{Foam}}{\varepsilon_{Foam}} + x(t)}{A\varepsilon_0}\times$$
$$e^{-\int_0^t \frac{\frac{d_{Foam}}{\varepsilon_{Foam}}+x(\tau)}{A\varepsilon_0 R_L}d\tau}\int_0^\tau\left(\frac{F\varphi_{Foam}}{3eAE'}\sqrt{\frac{\pi}{m_2}}\left(1+\sqrt{1+\frac{\dot{x}(\tau)^2}{g\delta_{st}}}\right)\right)e^{\int_0^\tau \frac{\frac{d_{Foam}}{\varepsilon_{Foam}}+x(z)}{A\varepsilon_0 R_L}dz}d\tau \quad (6)$$

From (6), once the structure of TEHs is fixed, the impact force F_e dominates the output voltage as shown in the simulation.

Next, we need to further consider the pairing capacitance. When adding the pairing capacitance, C_{pair}, the output voltage of the TEH can be derived from (4) and represented as (7). The difference of (7) and (4) indicates the influence of the pairing capacitance for triboelectric energy harvesting. Using the same method as (4)-(6), we can have an analytical solution of voltage generation considering pairing capacitance as (8).

$$V = -\frac{Q\left(d_{Foam}+\varepsilon_{Foam}x(t)\right)}{A\varepsilon_0\varepsilon_{Foam}+C_{pair}\left(d_{Foam}+\varepsilon_{Foam}x(t)\right)} + \frac{F\varphi_{Foam}}{3eAE'}\sqrt{\frac{\pi}{m_2}}\left(1+\sqrt{1+\frac{\dot{x}(t)^2}{g\delta_{st}}}\right) \quad (7)$$

$$V(t) = -\frac{F\varphi_{Foam}}{3eAE'}\sqrt{\frac{\pi}{m_2}}\left(1+\sqrt{1+\frac{\dot{x}(t)^2}{g\delta_{st}}}\right) -$$
$$\frac{d_{Foam}+\varepsilon_{Foam}x(t)}{A\varepsilon_0\varepsilon_{Foam}+C_{pair}\left(d_{Foam}+\varepsilon_{Foam}x(t)\right)}\times e^{-\int_0^t \frac{d_{Foam}+\varepsilon_{Foam}x(\tau)}{R_L\left(A\varepsilon_0\varepsilon_{Foam}+C_{pair}\left(d_{Foam}+\varepsilon_{Foam}x(\tau)\right)\right)}d\tau}\times$$
$$\int_0^\tau\left(\frac{F\varphi_{Foam}}{3eAE'}\sqrt{\frac{\pi}{m_2}}\left(1+\sqrt{1+\frac{\dot{x}(\tau)^2}{g\delta_{st}}}\right)\right)e^{\int_0^\tau \frac{d_{Foam}+\varepsilon_{Foam}x(z)}{R_L\left(A\varepsilon_0\varepsilon_{Foam}+C_{pair}\left(d_{Foam}+\varepsilon_{Foam}x(z)\right)\right)}dz}d\tau \quad (8)$$

With this new model, we can quantitatively analyze the contributing factors and understand their contribution to the output voltage of TEHs. This new model will then be used as the guideline for identifying the typical waveforms of TEHs. From (6) and (8), the output voltage of the TEH is determined by different contributing parameters mainly including the dynamic contact force in practical condition and the proposed pairing capacitance. The influence of these two contributing factors are clear as shown in Fig. 4 (a) and (b), which is the numerical analysis conducted using MATLAB. The theoretical output voltage is plotted. With the change of the impact factor (*i.e.*, the impact force), the output voltage changes not only its amplitude but also the waveform. The impact factor causes the frequency shift of the voltage output. The pairing capacitance mainly affects the amplitude of the output voltage theoretically. The detailed simulation and experimental validation and the results will be presented in Sections IV.B and IV.C theoretically. With the validation, this model will further be used to design the SSHI interface as identifying peaks of the TEH output voltage and source capacitance of harvesters is the key in the SSHI design. The model quantitatively shows the typical waveform and the effect of the pairing capacitance.

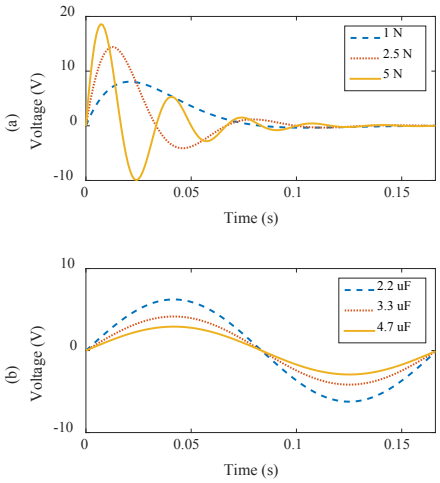

Fig. 4. Theoretical solution of output voltage of TEHs in one cycle. Effects of changing (a) the impact force and (b) the pairing capacitor on the voltage output of TEHs.

III. Proposed SSHI Rectifier

A. Proposed SSHI Circuit

Bridge rectifiers are simple and effective for ac-dc conversion for most mechanical energy harvesters. This type of rectifiers, however, cannot ensure the energy flow direction during certain intervals in each cycle, which may result in energy returns from the electrical part to the mechanical part [26]. SSHI rectifiers interfacing with harvesters is capable of overcoming this energy-returning problem in piezoelectric energy harvesting by introducing an inductive switch path in which an inductor and a switching component are added either in parallel or in series to the bridge rectifier. According to whether parallel or series, SSHI rectifiers can be divided into two categories, p-SSHI, and s-SSHI. Both have been successfully implemented for piezoelectric energy harvesting with a variety of existing studies [27]-[38]. SSHI rectifiers minimize the energy dissipation on the source capacitance of harvesters by controlling the optimal timing of switching approaches to match the LC loop formed by the added inductor and the source capacitance. By using these SSHI rectifiers, piezoelectric energy harvesting systems can achieve higher energy efficiency for mechanical energy conversion.

In this study, we successfully develop an SSHI rectifier for triboelectric energy harvesting. Comparing to simply using the conventional bridge rectifier as illustrated in Fig. 5 (a), we develop a p-SSHI rectifier interfacing with the TEHs as the

This article has been accepted for publication in a future issue of this journal, but has not been fully edited. Content may change prior to final publication. Citation information: DOI 10.1109/TPEL.2019.2934676, IEEE Transactions on Power Electronics

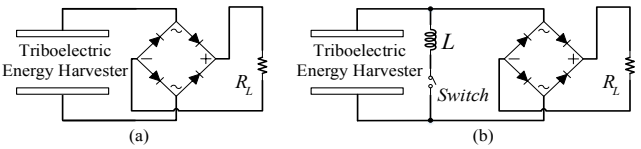

Fig. 5. Equivalent circuits for managing power of TEHs: (a) A full-wave bridge rectifier; (b) adding an SSHI interface.

power management circuit. The equivalent circuit model is shown in Fig. 5 (b). Fig. 6 illustrates the detailed circuit of the proposed SSHI interface. Previously we proposed an equivalent circuit model for TEHs [25] in which a current source $d\Delta Q / dt$ is in parallel to the changeable air layer C_{air} and then in series to other layers, such as C_{Foam} in this case. This is because when capacitors are connected in series, each of them stores an instantaneous charge equal to each other. As described in Section II.B, the original TEH is then parallel to the pairing capacitor C_{pair}. In Fig. 6, R_T is the inner resistance of the TEH which is negligible in this case. The dash line circles equivalent circuit model of our TEH with consideration of the source capacitance design. i_T is the output current of the overall TEH. When using a bridge rectifier, this output current will charge the source capacitance of the harvester first before it can flow to the output in every half cycle. The proposed p-SSHI interface circuit contains an inductor and a switch in parallel to the TEH. The switching circuit, in this case, consists of a pair of n-MOSFETs in a symmetric structure which ensures the switching process working properly for both positive and negative peaks. The MOSFETs are low energy consumption during switching. The interface circuit then connects to a bridge rectifier. R_L is the load.

B. The Operation

In the contact-separation mode of triboelectric energy harvesting, the charge is generated when the two TEH plates contact each other and then redistributed when the separation distance increases. In the analysis, we assume one plate is fixed whereas the other is movable to achieve contact and separation. Thus we also use displacement for separation distance.

Due to the periodic contact and separation between the plates with a sinusoidal separation distance as shown in Fig. 7 (a), the TEH output voltage with or without the SSHI interface are periodic as well with the same period. In the displacement plot in Fig. 7 (a), the negative peaks refer to the contact point of the two plates whereas the positive peaks refer to the maximum separation distance. In the experiment, an accelerometer is attached is the fixed plate to monitor the effect of the impact force. The signal from the accelerometer is shown in Fig. 7 (b). The output voltage is affected by the impact force and the following interfacing circuit, which shows high nonlinearity from the displacement input. This is different from the other three types of mechanical energy harvesting.

Here we use one single period from t_0 to t_3 as marked in Fig. 7 (d) to analyze the operation of the TEH first. In each cycle of the input sinusoidal movement, the two layers start to physically contact each other before the displacement reaches its minimum due to the thickness of the foam layer. This

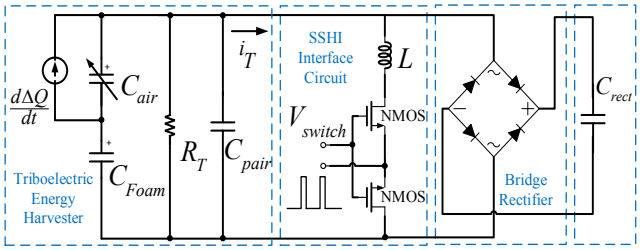

Fig. 6. Proposed SSHI interface circuit.

contacting time point is defined as t_0. Before t_{0-} the two TEH plates are separated and the movable plate moves towards the fixed plate. After t_{0+}, the movable plate continues moving until the displacement reaches its minimum that the foam layer is compressed till the minimum thickness as the negative peaks in Fig. 7 (a). When the two places physically contact, the impact force occurs and a pulse is generated from the accelerometer as shown in Fig. 7 (b). During the physical contact, due to the triboelectric effect, the charge is generated on the contacting surfaces of the two triboelectric material layers. In this study and other theoretical analyses for triboelectric energy harvesting, the charge is assumed to be evenly distributed with a surface charge density σ. Then the movable plate changes its moving direction and the two layers begin the separation. When the separation physically occurs, the potential difference of the two electrodes emerges and drives the electrons to flow through the external circuit (e.g. a load resistor for oscilloscope). The output voltage (i.e. the voltage through the load resistor) reaches the maximum (positive peaks in Fig. 7 (d)) at the time t_1 and then decreases during the separation. After the plates separate from t_1, the potential difference between the two plates decreases with the diminished charge density. The voltage reaches its minimum at t_2 as the negative peaks in Fig. 7 (d). The two plates keep separating and their distance increases till the maximum. The output voltage of the TEH changes from negative to positive at t_3 which is the starting of the next cycle when the two plates start to physically contact again. When there is no pairing

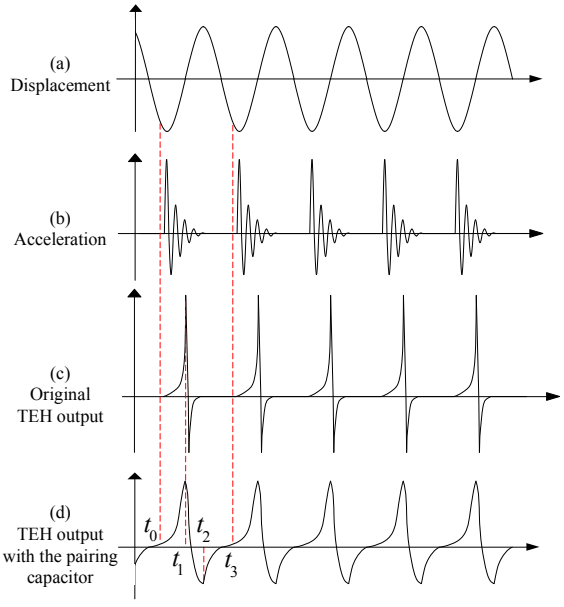

Fig. 7. Typical waveforms of TEHs. (a) Displacement; (b) acceleration; (c) TEH voltage with changeable capacitance; (d) TEH voltage with pairing capacitance.

This article has been accepted for publication in a future issue of this journal, but has not been fully edited. Content may change prior to final publication. Citation information: DOI 10.1109/TPEL.2019.2934676, IEEE Transactions on Power Electronics

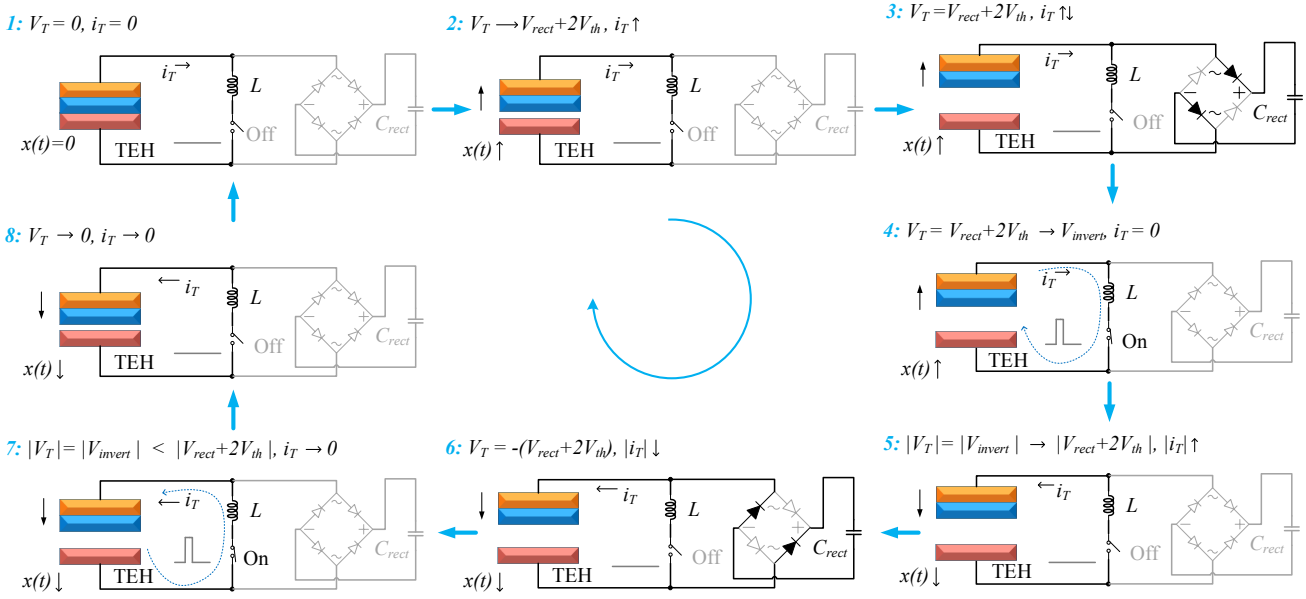

Fig. 8. The schematic diagrams of the operation and physical process with the circuitry analysis.

capacitor, the charge flow through the external circuit quickly ends, which acts as a high electrical pulse. The movable plate repeats the motion as that from time t_{0+} to time t_{3-} as one cycle. The schematic diagrams of the physical process with the circuitry analysis have been represented in Fig. 8. During the entire process, the source current, i_T, in the TEH is shown in Fig. 9 (a).

When there is a full-wave bridge rectifier with a smoothing capacitor C_{rect}, the rectifier voltage V_{rect} is ideally dc but with ripples. The ripples are mainly determined by the smoothing capacitance and can be negligible when the capacitance is large. Firstly, we assume that V_{rect} is dc as in the ideal case. In the analysis, we make an assumption that the source capacitance with the added pairing capacitance from the TEH

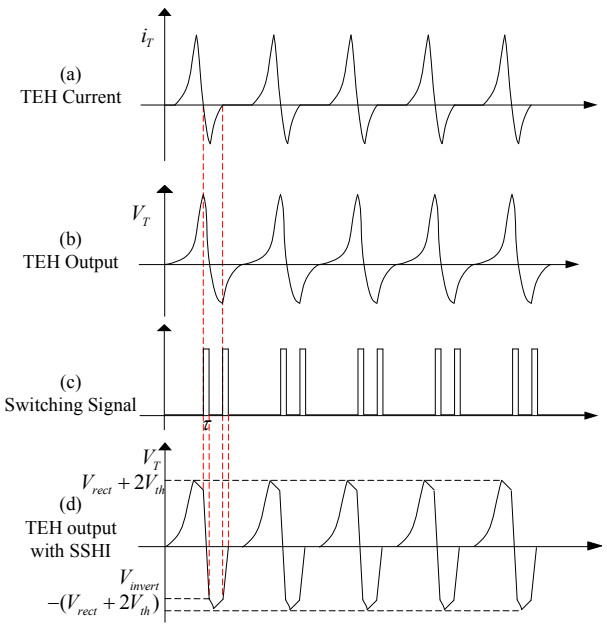

Fig. 9. Typical waveforms of the SSHI rectifier circuit. (a) The TEH current; (b) the TEH voltage without the SSHI interface; (c) switching signals; (d) the TEH voltage with the SSHI interface.

multilayer structure is independent and stable from the mechanical motion. In the operation, the source current i_T needs to charge the harvester capacitance C_T until it reaches $|V_{rect}+2V_{th}|$ so that the bridge conducts, and then $|V_T| = |V_{rect}+2V_{th}|$. When i_T changes the direction and $|V_T| < |V_{rect}+2V_{th}|$ again, the load side and the harvester side are isolated. In triboelectric energy harvesting, the source current i_T can seldom be sinusoidal due to the high nonlinearity between the displacement and the charge generation as analyzed in our model in Section II.C. Also unlike piezoelectric energy harvesting that has a steady current source resulted from continuous mechanical input, the source current i_T in triboelectric energy harvesting not always exists in every cycle as shown in Fig. 9 (a). The voltage of the TEH, V_T, either varies following the current i_T or equals to $V_{rect}+2V_{th}$, depending on whether the bridge conducts. When isolated, the current needs to charge the harvester capacitance C_T until the next bridge conduction. Thus, a considerable amount of energy is dissipated on the source capacitance. Also in some conditions of triboelectric energy harvesting, the negative voltage peaks are not high so that they cannot make the bridge conduct, although the positive peaks are mostly high enough. In addition, when considering the ripples of V_{rect} and the short conducting time in each cycle, there may not be a perfect steady duration in the TEH voltage waveform V_T. A typical waveform of the TEH voltage with a bridge rectifier is shown in Fig. 9 (b).

When adding the designed SSHI interface with the optimal switching-on time, the LC loop which consists of the source capacitance of the TEH C_T and the inductor in the SSHI interface L is able to flip the voltage quickly instead of charging the source capacitance at each zero-crossing point of the source current i_T, which reduces the energy return to the harvester and enhances the energy efficiency in the rectifier stage. The schematic diagrams of the operation and physical process are illustrated as Steps 1-8 in Fig. 8. In the initial

This article has been accepted for publication in a future issue of this journal, but has not been fully edited. Content may change prior to final publication. Citation information: DOI 10.1109/TPEL.2019.2934676, IEEE Transactions on Power Electronics

condition, it is assumed that $V_T = 0$ and $i_T = 0$. The operation starts with the first contact of the two triboelectric layers as Step 1. In the operation, the source current i_T of the TEH is generated by physical contact and separation process. In each cycle, this current needs to charge the harvester capacitance C_T until it reaches $|V_{rect} + 2V_{th}|$ before the bridge is able to conduct. When the harvester voltage reaches $|V_T| = |V_{rect} + 2V_{th}|$, the bridge conducts as Steps 2 and 3. In the equivalent circuit as Fig. 5 (b), the switch in the inductor path is controlled to be closed at each zero-crossing point of the current i_T as Step 4 with the switch controlling signal shown in Fig. 9 (c). At this moment, the current i_T changes its direction, and the switch instantly turns on. The harvester side is an LC circuit and will quickly flip V_T to $-V_{invert}$ in Step 5. $|V_T|$ is lower than the rectifier voltage $|V_{rect}|$ plus $2V_{th}$, and the bridge is not conductive. The current i_T will charge C_T for a short time until $|V_T| = |V_{rect} + 2V_{th}|$. This charging time is much less than that without the inductor. Then the bridge will conduct again and i_T flows to the load side from the other pair of diodes as Step 6. In triboelectric energy harvesting, the source current i_T does not always exist in one cycle as shown in Fig. 9 (a) because the charge transfer may be much faster than the mechanical vibration because the mechanical input is a low frequency in this case (i.e. 6 Hz). This low-frequency triboelectric energy harvesting can be applied in a number of application scenarios such as human motion, wind-induced motion, etc. Thus, the TEH voltage goes to zero in between cycles as Steps 7 and 8. Also as mentioned above, sometimes the negative voltage peaks are not as high as the positive peaks, and the bridge rectifiers sometimes cannot flip the negative peaks as shown in the Fig. 9 (b) and validation experiment (e.g. Fig. 16 (d)). When using LC resonance to flip voltage, the negative peaks can be as high as positive peaks as shown in Fig. 9 (d), which is also validated in the experiment as shown in Fig. 16 (e). This will further enhance energy efficiency for triboelectric energy harvesting comparing to adopting bridge rectifiers.

During the operation, the switching process needs to be conducted quickly. The key to success is the timing of the switch. Generally, the time interval of switching-on, τ, is optimized to be half period of the LC loop, which is $\tau = \pi\sqrt{LC_T}$. It is usually only tens or hundreds of microseconds when adopting a small inductance.

C. V-Q Plot Analysis

TENGs or TEHs are emerging since 2012 and have had promising progress in recent years. A standard method which is the plot of built-up voltage V versus total transferred charges Q (V-Q plot) of harvesters was first proposed in 2015 to quantitatively evaluate the performance of TENGs [43], which provides a performance figure-of-merit for each cycle of motion. This method was further well applied to evaluate the performance with energy storage elements in their following study [44]. TENGs have four modes generated by either sliding motion or contact and separation. Zi *et al*. [44] analyzed the physical process of the direct charging cycle and developed the corresponding V-Q plot of sliding mode which can achieve symmetrical positive and negative peaks. Fig. 10 (a) and (b) are the V_T - t plot and the V-Q plot for sliding mode with a bridge rectifier and load capacitance with the corresponding typical time points (as III, IV, V, VI) labeled in both sub-figures. The energy output of TENGs per cycle is the boxed area [43].

For contact-separation mode as studied in this case, the positive and negative peaks are often not symmetrical, which is also observed in some other studies [45]-[47]. In some cases, the absolute amplitude of negative peaks are much lower than that of positive peaks and sometimes cannot make the bridge conduct in the negative half cycle. In this case, the corresponding V_T - t plot and the V-Q plot are shown in Fig. 10 (c) and (d). The harvester output energy with a bridge rectifier per cycle in stable cycles is also the boxed area and can be calculated as (9),

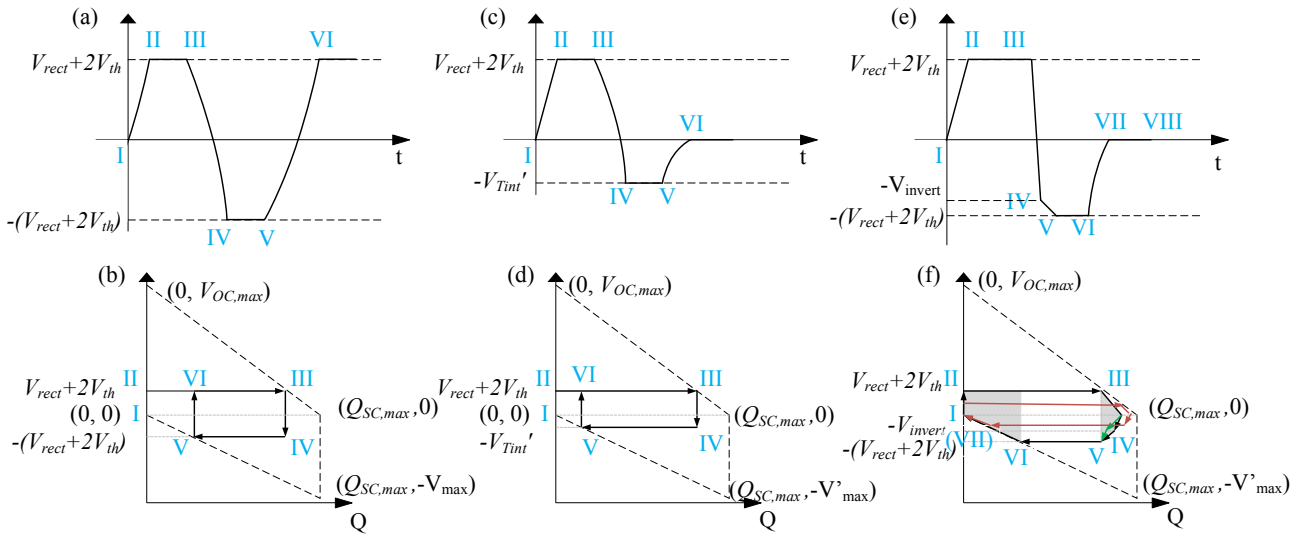

Fig. 10 (a) V_T-t plot and (b) V-Q plot of sliding mode [44]; (c) V_T-t plot and (d) V-Q plot of contact-separation mode of the TEH with a bridge rectifier; (e) V_T-t plot and (f) V-Q plot of the TEH with the designed SSHI rectifier. (Black lines are stable cycles in all three cases; red line refers to unstable cycles in (f).)

This article has been accepted for publication in a future issue of this journal, but has not been fully edited. Content may change prior to final publication. Citation information: DOI 10.1109/TPEL.2019.2934676, IEEE Transactions on Power Electronics

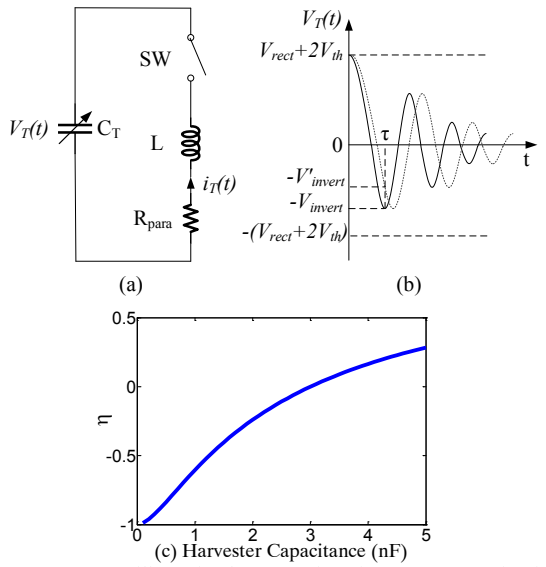

Fig. 11. RLC oscillator in the SSHI interface. (a) RLC circuit; (b) harvester capacitor voltage with the consideration of switching timing and pair capacitance design; (c) η ratio versus capacitance mismatching.

$$E_{Br} = \left(V_{rect} + 2V_{th} + V_{T\,\mathrm{int}}'\right) Q_{SC,\max} \times \left[1 - (V_{rect} + 2V_{th}) / V_{OC,\max} - V_{T\,\mathrm{int}}' / V_{\max}'\right] \tag{9}$$

where $Q_{SC,\max}$ is the maximum short-circuit transferred charge, $V_{OC,\max}$ is the maximum open-circuit voltage at Q=0, $V_{\max}'$ is the maximum achievable absolute voltage at $Q = Q_{SC,\max}$. $V_{\max}'$ in the contact-separation mode is much lower than that in sliding mode. The inverted voltage $-V_{T\,\mathrm{int}}'$ here refers to the maximum negative voltage the contact-separation mode can achieve.

When adding an SSHI rectifier for the contact-separation mode, the V_T charging process is significantly reduced due to the LC loop. The LC oscillation circuit on the harvester side is able to quickly flip V_T to $-V_{invert}$. The voltage $-V_{invert}$ is determined by how well the LC resonance can flip the voltage, which results from the optimization of switching. The working process of the TEH with an SSHI rectifier in each cycle is illustrated in Fig. 8 and the detailed analysis is described in Section III.B. The corresponding V_T - t plot and the V-Q plot within one cycle are shown in Fig. 10 (e) and (f) with typical time points (I-VII) labeled. The transitions between time points I-VII correspond to Steps 1-8 illustrated in Fig. 8. The harvester output energy per cycle is also the boxed area. Comparing with that with a bridge rectifier, the improved harvested energy per cycle on the harvester side can be approximately calculated by (10) assuming that the harvester voltage is fully flipped in each cycle and the negative half cycle can also achieve $V_{rect} + 2V_{th}$ as Fig. 10 (a),

$$E_{saved} = E_{SSHI} - E_{Br} = \frac{3}{2} Q_{SC,\max} (V_{rect} + 2V_{th})^2 / V_{\max}' + (Q_{LC} - Q_{SC,\max}(1 - \frac{V_{rect} + 2V_{th}}{V_{OC,\max}})) \cdot (V_{rect} + 2V_{th}) \tag{10}$$

which is the shaded area in Fig. 10 (f), where Q_{LC} is the charge level achieved by the LC oscillation. The V-Q plot of the TEH with a bridge rectifier and an SSHI rectifier is then validated in Section IV.F. The energy saving ratio λ in the percentage form can be then calculated by (11),

$$\lambda = \frac{E_{Saved}}{E_{Br}} = \frac{3Q_{SC,\max}\frac{V_{rect} + 2V_{th}}{V_{\max}'} + 2(Q_{LC} - Q_{SC,\max}(1 - \frac{V_{rect} + 2V_{th}}{V_{OC,\max}}))}{4Q_{SC,\max}(1 - \frac{V_{rect} + 2V_{th}}{V_{OC,\max}} - \frac{V_{rect} + 2V_{th}}{V_{\max}'})} \tag{11}$$

Thus, in each cycle, the saved energy using an SSHI rectifier is determined by the performance of the TEH and the LC oscillation. With the existing TEHs, the maximum and minimum energy saving ratio achieved by adding an SSHI happens at $Q_{LC} = Q_{SC,\max}$ and $Q_{LC} = Q_{SC,\max}\rho$, respectively, as shown in Fig. 10 (f). Let $\rho = 1 - (V_{rect} + 2V_{th}) / V_{OC,\max}$ and $p = (V_{rect} + 2V_{th}) / V_{\max}'$, the maximum and minimum energy saving ratio can be estimated as

$$\lambda_{\max} = \frac{3p - 2\rho + 2}{4\rho - 4p}, \quad \lambda_{\min} = \frac{3p}{4\rho - 4p} \tag{12}$$

Thus, the maximum energy saving ratio can reach up to 200% if the TEH is well designed. The minimum energy saving ratio can also achieve up to 50% in stable cycles.

When considering the difference between the maximum invertible voltage $-V_{invert}$ and $-(V_{rect} + 2V_{th})$ that results from the parasitic resistance of the LC loop and the non-optimized switching, the V-Q plot will be the green lines in Fig. 10 (e). The energy difference between the optimal and non-optimized cases is caused by charging the harvester capacitance from $-V_{invert}$ to $-(V_{rect} + 2V_{th})$ to conduct the bridge.

During low-frequency motion, there are also unstable cycles for energy harvesting. When the harvester with a bridge rectifier is under unstable cycles, the output voltage of the rectifier V_{rect} is not saturated and keeps increasing. Thus, the boxed area in Fig. 10 (d) keeps changing and intersecting with the two dash lines. The detailed analysis is well explained in [44]. For unstable cycles of SSHI rectifiers, the instability comes from two reasons. One is that the output voltage of the rectifier V_{rect} cannot achieve saturated at the beginning, which is similar to that with a bridge rectifier. In this situation, the physical process of the energy harvester with the SSHI stays the same and thus a typical unstable cycle in the V-Q plot is shown as red in Fig. 10 (f). The energy saving ratio as (11) and (12) is lower in this case as it is calculated as the shaded area over the boxed area in Fig. 10 (f). The other issue is that unstable cycles may result from motion instability and will cause mismatching of the LC oscillator. In this case, there is charge loss on the harvester capacitance and cannot achieve a high Q_{LC}. Thus, the shaded area on the right side in Fig. 10 (f) will become smaller, which means the energy saving ratio is lower.

D. Optimal Switching Design and Pair Capacitance

When designing SSHI rectifiers for triboelectric energy harvesting, the optimal switching-on time is critical. To discuss the switching optimization, we need to carefully consider the RLC circuit which is composed by the source capacitance C_T, the inductor L, and the cumulative parasitic resistance R in the loop that results from the inductor and the switch as shown in Fig. 11 (a). When the switch is closed during zero-crossing of i_T, the RLC circuit becomes a closed

This article has been accepted for publication in a future issue of this journal, but has not been fully edited. Content may change prior to final publication. Citation information: DOI 10.1109/TPEL.2019.2934676, IEEE Transactions on Power Electronics

loop and starts to oscillate immediately. During the switching-on time τ, the capacitor voltage can be calculated as [32],

$$v_T(t) = -\frac{\omega_0}{\omega_d}\left(V_{rect} + 2V_{th}\right)e^{-\alpha t}\cos\left(\omega_d t - \varphi\right) \tag{13}$$

where $\omega_d = \sqrt{\omega_0^2 - \alpha^2}$, $\omega_0 = \frac{1}{\sqrt{LC_T}}$, $\alpha = \frac{R_{para}}{2L}$, $\varphi = \cos^{-1}\left(\frac{\omega_d}{\omega_0}\right)$. If τ is selected as half of the period of $\frac{2\pi}{\omega_d}$, the flipped voltage will quickly achieve the half-period negative peak after τ as shown in Fig. 11 (b), which is [32],

$$V_{invert} = \left(V_{rect} + 2V_{th}\right)e^{-\frac{\pi}{2\sqrt{Q_F^2 - \frac{1}{4}}}} \tag{14}$$

where Q_F is the quality factor of the RLC loop, $Q_F = \frac{1}{R_{para}}\sqrt{\frac{L}{C}}$. In this case, the energy in the RLC circuit is quickly bounced back to the harvester capacitance by the inductor and dissipated by a very small amount on the small parasitic resistance.

For triboelectric energy harvesting, selecting the optimal switching time is much more challenging due to the real-time changeable harvester capacitance and the high non-linear terms in voltage and current calculation from a sinusoidal distance, which is different from piezoelectric energy harvesting. Also, as the RLC circuit with changing capacitance in Fig. 11 (a), the governing equation becomes non-linear and thus does not have an analytical solution for $v_T(t)$. As the designed switching-on time is fixed as $\tau = \pi\sqrt{LC_T}$, a small change of harvester capacitance ΔC in the RLC circuit will cause the inverted voltage decrease from (14) which can be estimated as (15) as shown in Fig. 11 (b),

$$V_{invert}' = -\frac{\omega_0'}{\omega_d'}\left(V_{rect} + 2V_{th}\right)e^{-\frac{\alpha}{\pi\omega_d}}\cos\left(\frac{\pi\omega_d'}{\omega_d} - \varphi'\right) \tag{15}$$

where,

$$\omega_d' = \sqrt{\omega_0'^2 - \alpha^2},\ \omega_0' = \frac{1}{\sqrt{L(C_T + \Delta C)}},\ \alpha = \frac{R_{para}}{2L},\ \varphi = \cos^{-1}\left(\frac{\omega_d'}{\omega_0'}\right) \tag{16}$$

where $C_T = C_{pair} + \frac{\varepsilon_0 A C_{Foam}}{\varepsilon_0 A + C_{Foam}x(t)}$ in our design. ΔC is caused by $x(t)$ changing during the switching time duration or measurement error of the pair capacitance.

Here, we define η as the ratio of $-V_{invert}'/\left(V_{rect} + 2V_{th}\right)$ which is determined by the designed timing and the pair capacitance; thus,

$$\eta = -\frac{\omega_0'}{\omega_d'}e^{-\frac{\alpha}{\pi\omega_d}}\cos\left(\frac{\pi\omega_d'}{\omega_d} - \varphi'\right) \tag{17}$$

where $-1 \le \eta \le 1$. In the ideal case with zero parasitic resistance and exact matching capacitance, the η ratio is -1. When the pair capacitance is low, a small change of $x(t)$ causes a large change of C_T and thus leads to a small η ratio as shown in Fig. 11 (b) that $\left|V_{invert}'\right|$ is much lower than $\left|V_{rect} + 2V_{th}\right|$. In this case, even a small capacitance mismatching will cause η away from -1 which means that the voltage cannot be fully flipped due to the LC resonance. Thus, the major energy loss caused by the harvester capacitance in the full-bridge rectifier condition is still not solved. On the other hand, this pair capacitance can also decrease the TEH output voltage as analyzed in Section II.C, which aligns with the results in [22]. Thus in our design, we choose the minimal pair capacitance that can stabilize the harvester capacitance to achieve an optimal switching-on time. The validation experiments of optimal switching-on time are demonstrated in Section IV.G.

E. Harvested Power Estimation

Using the V-Q plot, we are able to estimate the output energy of the TEH. We then quantitatively estimate the saved harvested power by using SSHI rectifiers compared to simply using bridge rectifiers on the load capacitor side. With the SSHI interface, the energy efficiency is theoretically enhanced by lowering energy dissipation on the source capacitance as well as saving energy in low-level negative peaks as described in Section III.B.

In one steady cycle, with a bridge rectifier, the charge loss on the source capacitance C_T of the harvester occurs when charging the source capacitance C_T from $-(V_{rect} + 2V_{th})$ to $V_{rect} + 2V_{th}$ or vice versa [30]. With an SSHI rectifier, the charging process is significantly shortened by the LC oscillator flipping and occurs in the beginning of each cycle from 0 to $V_{rect} + 2V_{th}$ and from $-V_{invert}$ to $-(V_{rect} + 2V_{th})$ after LC oscillator flipping to the opposite direction. Comparing with using a bridge rectifier, the saved charge loss can be expressed as,

$$\begin{aligned} Q_{C_T,loss} &= 2\left(V_{rect} + 2V_{th}\right)C_T - \left(V_{rect} + 2V_{th} - V_{invert}\right)C_T \\ &= \left(V_{rect} + 2V_{th} + V_{invert}\right)C_T \end{aligned} \tag{18}$$

where V_{invert} is shown in Fig. 9 (d).

Also, the charge loss on the internal resistance of the TEH in every cycle is simply $Q_{R_T,loss} = \int_0^T \frac{V_T}{R_T}dt$. As the inner resistance of the TEH R_T is very large, the charge loss on the inner resistance can be negligible.

The total charge produced by the TEH in every cycle is:

$$Q_{total} = \int_0^T \left|i_T\right| dt \tag{19}$$

And i_T can be calculated from (7) and (8) as dQ/dt, which is generated by triboelectric energy harvesting.

Therefore, the harvested power of the circuit with the SSHI interface for every cycle is:

$$P_{harvest} = V_{rect}\left(\frac{Q_{total} - Q_{C_T,loss}}{T}\right) \tag{20}$$

The difference between the full-wave bridge rectifier and the circuit with the designed SSHI interface of the harvested power comes from the inverted charges due to the switching

This article has been accepted for publication in a future issue of this journal, but has not been fully edited. Content may change prior to final publication. Citation information: DOI 10.1109/TPEL.2019.2934676, IEEE Transactions on Power Electronics

approach as (9). Therefore, the saved power comparing to only using a bridge rectifier, P_{saved} , can be calculated as

$$P_{saved} = V_{rect}\frac{(V_{rect} + 2V_{th} + V_{invert})C_T}{T} \tag{21}$$

In some cases that the negative voltage peaks are not high enough to make bridge conduct, more power can be saved when using SSHI. In this case, the saved power can be estimated as

$$P_{saved} = V_{rect}\left(\frac{Q_{C_T,loss} + Q_{N,loss}}{T}\right) \tag{22}$$

where $Q_{N,loss}$ is the charge loss caused by the non-conduction of the bridge during the negative period of the TEH voltage.

IV. Experiments and Results

In this section, the experiments and results for validating the new theoretical model of triboelectric energy harvesting and the proposed SSHI rectifier are both presented. The experiment platform for generating the sinusoidal distance and measuring necessary signals is established as shown in Fig. 12.

A. Experimental Platform and Setup

In order to achieve a sinusoidal separation distance of the two TEH plates for validation experiments, we first build an experiment platform that is capable of providing continuous sinusoidal movements. The details of the system are illustrated in Fig. 12 (a). The structure is mainly built based on a linear actuator and the mechanical design of a slider-crank mechanism [39]. A movable plate is mounted on the slider, which is connected to a coupler via a revolute joint and driven by a stepper motor. The frame and the wheels of the linear actuator are 3D printed using carbon fiber nylon to provide a strong and light structure. An IR distance sensor (GP2Y0A21, Sharp Inc.) is equipped to monitor the displacement in real time. A reflection plate is coupled with the distance sensor. To measure the impact force during the two plates contacting, an accelerometer (±50 g, 353B33, PCB Piezotronics Inc.) is attached to the fixed plate to measure the generated acceleration signal during contacting as the fixed plate is generally stable except when two plates contact.

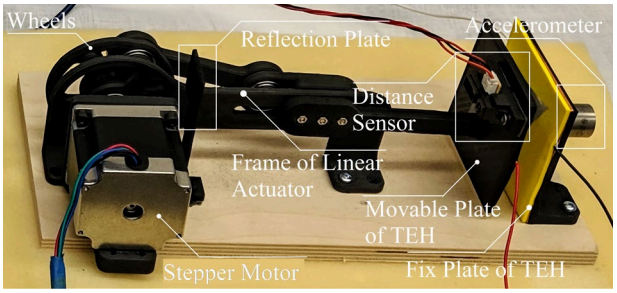

(a)

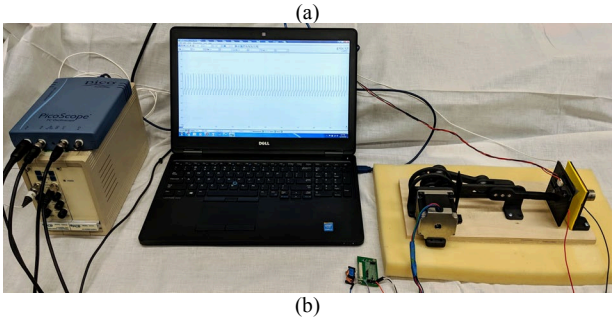

(b)

Fig. 12. Experimental setup. (a) Linear actuator with sensors that can generate sinusoidal displacement of the TEHs; (b) the entire experimental setup.

TABLE I
Parameters of Components in the Circuit

Variable	Value
C_{tribo}	0 – 15 nF
C_{pair}	49.95 nF
C_T	49.95 – 64.95 nF
L	100 mH
R_L	10 MΩ
C_{rect}	2.2, 10, 47, 470 μF
f_T	6 Hz
τ	222 μs

The experimental setup is shown in Fig. 12 (b). The linear actuator is mounted on the wood board with a foam pad to stabilize the movement. The displacement and acceleration signals are monitored and stored in a laptop via an oscilloscope (PicoScope 4424, Pico Technology Inc.). This platform is capable of providing sinusoidal separation distance for TEHs as the controllable mechanical input and recording the necessary signals for validation experiments. Table I summaries the parameters in the circuit used in the experiments.

B. Simulation Results for the Proposed Model of Triboelectric Energy Harvesting

For conventional mechanical energy harvesting, three mechanisms are generally used, which are piezoelectricity based on piezoelectric materials, electromagnetics based on Lenz's Law, and electrostatics based on variable capacitance [40], [41]. For analyzing these processes of energy conversion, sinusoidal forces are typically considered as mechanical input. For typical piezoelectric or electromagnetic energy conversion, the displacement or distance $x(t)$ and the generated source voltage $V(t)$ of harvesters are usually sinusoidal as well. This is because of the basically linear relationship between the displacement and the input force or vibration in these harvesting models although nonlinear terms also exist [28]. Although there could be a slight misalignment between theoretical models and experimental results, the output voltage is generally sinusoid with damping, phase shift and other slight modification comparing to the input waveform. However, in triboelectric energy harvesting, a sinusoid motion input generally cannot generate a sinusoid voltage across the two electrodes. Although a few studies have discussed the reason [23], [24], it is also likely that the impact force dominates the generated charge as our analysis in Section II.C and equations (6) and (8).

We then conduct the numerical simulation of our proposed model and the corresponding experiments to validate the model. In the simulation, a sinusoid waveform is set as the input separation distance between the two TEH layers (also called displacement of the movable plate) of the TEH. Assume that the input displacement is $x(t) = D_{pp}sin(2\pi ft)$, where D_{PP} is the maximum displacement which equals to 25 mm in the

This article has been accepted for publication in a future issue of this journal, but has not been fully edited. Content may change prior to final publication. Citation information: DOI 10.1109/TPEL.2019.2934676, IEEE Transactions on Power Electronics

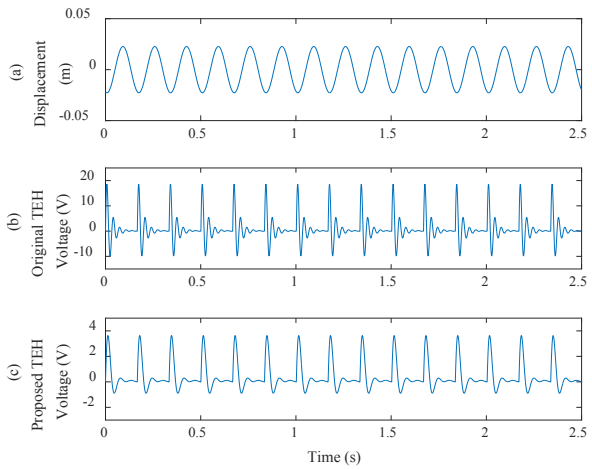

Fig. 13. The simulation results from MATLAB: waveforms of (a) the displacement, (b) output of the original TEH, and (c) output of the proposed TEH with the pairing capacitor. The waveforms of (b) and (c) are related to equations (6) and (8), correspondingly.

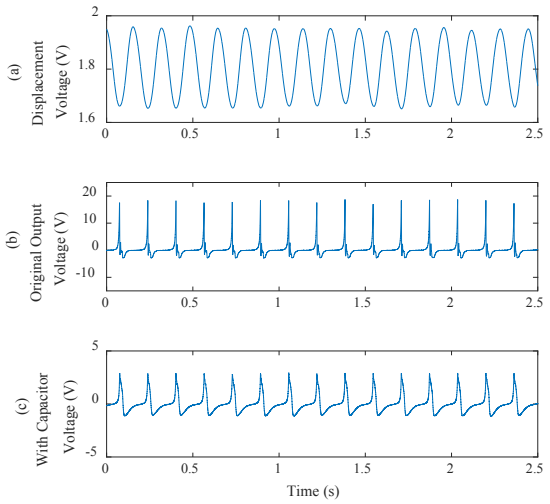

Fig. 14. Measured voltage in the validation experiments of the new model. Signals of (a) the displacement, (b) output of the original TEH, and (c) output of the proposed TEH with the pairing capacitor.

experiment setup, f is the frequency and $f = 6$ Hz which is to simulate the low-frequency movement. The waveform of the displacement is plotted in Fig. 13 (a). The smaller the displacement, the closer the two layers are. When the impact factor of the dynamic force is changed, it is dominant to both the amplitude and the waveform (*i.e.* frequency shift) of the output voltage of TEHs as shown in Fig. 4 (a). The higher the impact force is, the larger peaks the output voltage will achieve. When the impact factor (*i.e.* impact force) is higher and the contact and separation process is faster, the output voltage shows higher frequency with damping. When changing the input frequency, simulation results show that the influence of impact force is similar.

In order to clearly illustrate the difference between (6) and (8) (without and with pairing capacitor) in Section II.C, the solutions of the theoretical voltages have been derived in MATLAB and plotted as Fig. 13 (b) and (c). Table II summarizes the main parameters and the corresponding values in the simulation. By the new model as in (6), the theoretical voltage through TEH is plotted in Fig. 13 (b). With adding the pairing capacitor, the generated voltage of the TEH is plotted in Fig. 13 (c). After adding the pairing capacitor, the amplitude of voltage output of the TEH is decreased but the width of the peak wave is extended. From (8), the pairing capacitance which determines the switching time in the SSHI interface also influences the amplitude of output voltage of TEHs. Fig. 4 (b) shows the voltage with different values of pairing capacitance with the same other parameters. Higher pairing capacitance relates to lower voltage for the same impact force. In the real design of rectifiers, however, we also need to consider the switching time and the practical multilayer structure of the TEHs and therefore cannot use very small pairing capacitance in the real design. With the analytical solution of the output voltage of the TEH, we then conduct experiments to validate it.

C. *Validation Experiment and Results for Proposed Model of Triboelectric Energy Harvesting*

In the validation experiments, the sinusoid separation distance $x(t)$ is achieved by the experiment platform in Fig. 12 as the mechanical input. The frequency is also 6 Hz. The real displacement is measured by the IR distance sensor and the signal is plotted in Fig. 14 (a). During each cycle of the sinusoidal movement, a periodic signal is achieved. After the plates contact, the foam layer is pressed till having a minimum thickness. After a short period, the TEH output reaches its maximum value. Both positive and negative peaks are clearly shown in Fig. 14 (b) and (c), which are the measured voltage output of the TEH without and with adding the pairing capacitor, respectively. In Fig. 14 (b), the TEH output shows deep narrow positive and negative peaks as the theoretical voltage in Fig. 13 (b). The similarity also exists in the case by adding the pairing capacitor. In Fig. 14 (c), the positive and negative peaks of the TEH output are enlarged in terms of time, which corresponds to Fig. 13 (c). With a higher impact force, the positive voltage peak is always higher in the experiments as well. From the validation experiments, it shows that our proposed theoretical model aligns well with the experimental results.

D. *The TEH Performance*

Next, more experiments are conducted to evaluate the energy harvesting performance. First of all, the performance of the proposed low-cost easy-assembly TEH as co-designed for the proposed SSHI is estimated. In the experiment, the TEH with or without the proposed SSHI interface is applied to charge a load capacitor under a low-frequency periodic motion via the linear actuator. The experiment setup is described as Section IV.A. The load capacitors with different capacitance, 2.2 μF, 10 μF, 47 μF, and 470 μF, are used to quantitatively demonstrate the charging behavior under the input motion with the frequency of 6 Hz. The results with and without the SSHI interface are shown in Fig. 15 (a) and Fig. 15 (b), respectively. For all load capacitors, the saturation charging curves are observed. The charging speed gradually decreases along with time until the charging voltage reaches the maximum of approximately 1.3 V. For a 2.2 μF load capacitor, it takes 11.06 seconds to charge to 1.3 V. For a load capacitor with larger capacitance, it takes a longer time to reach its saturation voltage. It takes 58.06 seconds and 203.9

This article has been accepted for publication in a future issue of this journal, but has not been fully edited. Content may change prior to final publication. Citation information: DOI 10.1109/TPEL.2019.2934676, IEEE Transactions on Power Electronics

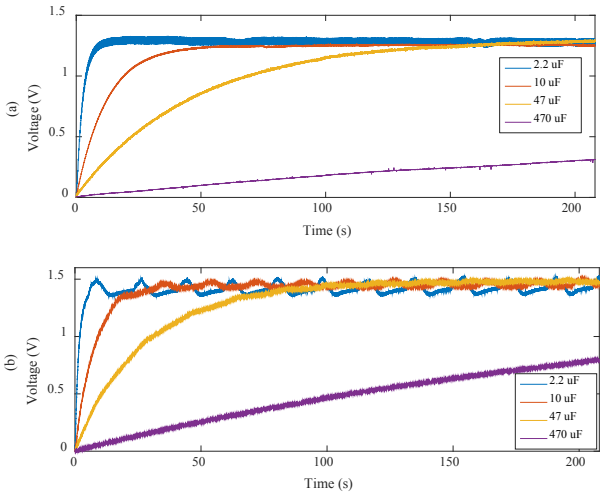

Fig. 15. Charging different capacitors with the proposed TEH (a) without and (b) with the proposed SSHI interface.

seconds for charging a 10 μF capacitor and a 47 μF capacitor to the saturation voltage, respectively. This demonstrates that our ultra-low-cost, easily-assembled TEHs can also achieve good results.

For comparison, the results of charging these capacitors with the proposed SSHI interface have been shown in Fig. 15 (b). The maximum charging voltage, in this case, is higher than 1.3 V, which is approximately 1.45 V. The rectifier voltage V_{rect} is ideally dc but with ripples. The ripples are mainly determined by the capacitance C_{rect} and the input frequency. It can be negligible when the capacitance is large. By comparing the charging curves in Fig. 15 (a) and Fig 15 (b), all the load capacitors can also be charged faster with the proposed SSHI interface. The time of charging from zero to saturation voltage for 2.2 μF, 10 μF, 47 μF capacitors is 8.51 seconds, 34.78 seconds, 101.70 seconds. When charging higher capacitance, the charging to saturation with the SSHI interface is much faster than that without the SSHI. For example, when charging a 47 μF load capacitor, it is half of the time of that without the SSHI. The experimental results show that the stored energy in the load capacitors of 2.2 μF, 10 μF, 47 μF is 1.949 uJ, 8.107 μJ, 40.364 μJ, and 29.173 μJ, respectively. With the proposed SSHI interface, the stored energy of those capacitors is 2.623 μJ, 11.790 μJ, 73.846 μJ. Therefore, the proposed SSHI interface can significantly improve the stored energy when charging different capacitors.

E. Experiment and Results for the Proposed SSHI Rectifier

In the design of the pairing capacitor C_{Pair} which is used to ensure that the source capacitance is within a controllable range, C_{Pair} is selected to be larger than the value of $C_{air} \parallel C_{Foam}$. The total capacitance of the TEH is designed to have a limit of 50 nF. The inductance L is 100 mH. Therefore, the optimal switching-on time is half of the period of the LC loop, which is 222 μs in this case.

In the experiments, the fixed plate keeps stable while the movable plate moves at a frequency of 6 Hz which is identical to the simulated input for the theoretical model. The switching signals have a frequency of 12 Hz and a period of 83.33 ms which is much longer than the switch-on time. The switching

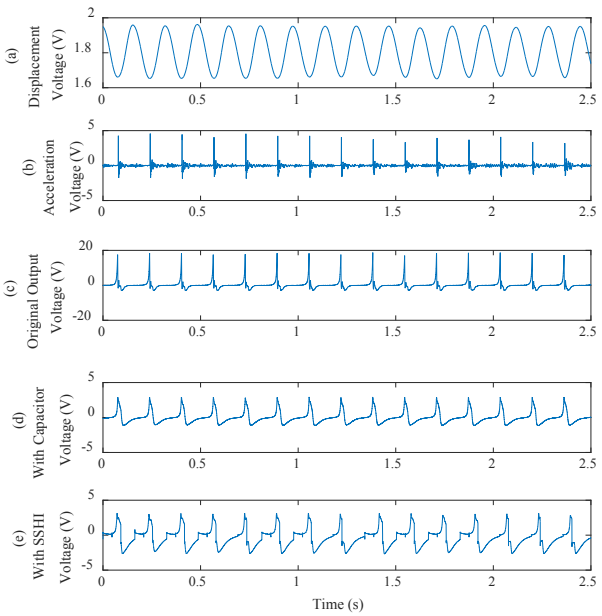

Fig. 16. Measured voltages in the experiments for validating the SSHI rectifier performance. (a) Displacement voltage detected by the IR distance sensor; (b) acceleration signal from accelerometer; (c) TEH voltage with no rectifiers or pairing capacitor; (d) TEH voltage with a bridge rectifier; (e) TEH voltage with the SSHI rectifier.

is turned on twice in one cycle when the voltage of the TEH reaches its positive and negative peak. This is because when the current i_T is zero crossing, the voltage V_T reaches its maximum. The synchronization of the switching interval and the extreme positions of the plate movements are critical to the power efficiency. If the switching-on occurs before or after the time point, the mechanical energy is hardly ensured to be optimized to transfer to the load. The switch is composed of a pair of n-MOSFETs to ensure the switching for both positive and negative peaks. The input impedance of the oscilloscope for measurements acting as the load resistance in the validation experiments is 10 MΩ. Four signals are measured and recorded, displacement of the movable plate by the IR sensor, the acceleration signal from the accelerometer, the output voltage of the TEH with a bridge rectifier and that with an SSHI rectifier.

The experiment results of the synchronized signals are illustrated in Fig. 16. Fig. 16 (a) shows the periodical signal of the displacement detected by the IR distance sensor, which shows that our platform using the slider-crank mechanism and linear actuator can generate a stable sinusoidal motion for experiments. The acceleration signal is plotted in Fig. 16 (b) to illustrate the contact force in each cycle. The original output of the TEH without the pairing capacitance is shown in Fig.

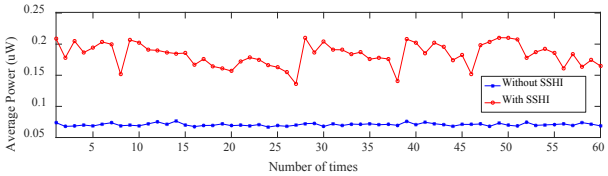

Fig. 17. Average harvested power of the proposed TEH with or without the SSHI interface circuit in 60 sets of experiments with the frequency of the input motion of 6 Hz.

This article has been accepted for publication in a future issue of this journal, but has not been fully edited. Content may change prior to final publication. Citation information: DOI 10.1109/TPEL.2019.2934676, IEEE Transactions on Power Electronics

16 (c). The output voltage ranges from -3 V to +19 V, which equals to a peak-to-peak voltage of 22 V. For the new TEH with the pairing capacitor added by the multilayer structure, the peak output voltage is lower whereas the effective area is wider.

The TEH voltage with a bridge rectifier and with the SSHI rectifier are measured for validation and plotted in Fig. 16 (d) and (e), representatively. The actual output of the SSHI interface aligns well with the theoretical analysis of the operation as shown in Fig. 9. In the measured TEH voltage with the SSHI rectifier, in the beginning, the voltage gradually increases to the peak. There is a very short slope down after the peak which may be the ripple of V_{rect}. Then the switch is quickly turned on, and the TEH voltage immediately flips to a negative value that is lower than the negative peak, which is V_{invert}. From V_{invert} to the negative peak, a charging process can be clearly observed from the measured TEH voltage waveform. Also, in this case, the negative peak of the TEH voltage with a bridge rectifier is not high and cannot conduct the bridge in the negative half as shown in Fig. 16 (d). Thus the TEH voltage in the negative half cannot reach $V_{rect}+2V_{th}$ and stay low. The LC loop in the SSHI rectifier seems to successfully flip the voltage and thus can achieve a much higher peak in the negative half and conduct the bridge in the negative cycle in Fig. 16 (e). This synchronized switching approach can boost up the harvested power. Thus, the measure results align well with our theoretical analysis.

We then measured and calculated the harvested power in the experiments by adding a load resistor. In order to estimate the energy enhancement of the proposed SSHI rectifier for the TEH compared with the commonly used bridge rectifiers in existing studies, the output power with and without the SSHI interface circuit is calculated and compared. The input for both cases is the same and is generated by the linear actuator and a step motor. The input power is approximately constant in the experimental platform. The average power in one cycle is calculated as

$$P_{avg}=\frac{1}{(t_3-t_0)}\int_0^T\frac{V_{rect}^2}{R_L}dt \tag{23}$$

In the experiments, 60 sets of experimental data have been recorded and analyzed. The average power harvested in the 60 sets of experiments with or without the proposed SSHI interface circuit is summarized in Fig. 17. In all the 60 experiments, the maximum output power of the TEH with the proposed SSHI interface circuit is always higher than that with a bridge rectifier. And it also occurs in the average harvester power as shown in Fig. 17. For both average power and maximum power, the ratio of the harvested energy without and with the SSHI interface can be up to 3.4283, which indicates that the harvested energy has been enhanced by up to 242.83%. This value shows that the proposed SSHI interface can significantly improve energy efficiency in triboelectric energy harvesting. In the implementation of switching, we cannot achieve the optimal timing of switching (i.e. exactly catching the zero-crossing of the current i_T) in every cycle due to the physical vibration in the real experiments; thus the power in every cycle is fluctuating somehow.

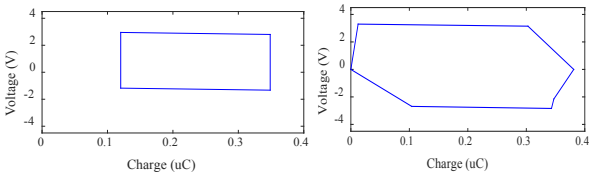

(a) (b)

Fig. 18 V-Q plot of the TEH energy output per cycle (a) with a bridge rectifier and (b) with the designed SSHI rectifier.

F. Results of V-Q Plot

To validate the V-Q plot analysis for the TEH output energy per cycle, a testing circuit with synchronized measurement of voltage and charge using Keithley 6514 is used in the experiment, which is the same as that in [44]. The performance of the TEH with a bridge rectifier and the designed SSHI rectifier is both evaluated. A smoothing capacitor of 10 μF is used in both experiments. When using the bridge rectifier, the positive charging voltage can be 2.95 V whereas the negative peak can only be -1.18 V in this case. The negative half cannot make the bridge conduct as it cannot reversely charge V_T to reach $-(V_{rect}+2V_{th})$. Thus, the measured V-Q plot is shown in Fig. 18 (a). When adding the designed SSHI rectifier, the measured V-Q plot is shown in Fig. 18 (b), in which the boxed area is the energy output in each cycle of the TEH. The positive peak voltage can achieve 3.30 V whereas the negative flipped voltage can achieve -2.69 V. In the experiment, the time duration of both positive and negative maximum voltage is not exactly flat, and the duration is not long either. Thus the measured V-Q plot is approximately close to the theoretical analysis but not the same.

G. Discussion of Switching

From the analysis in Section III.B and III.D, the timing and switching-on time τ are critical for successfully designing the SSHI rectifier for triboelectric energy harvesting. The switching timing needs to capture the zero-crossing of the current i_T. In the experiment, the total harvester capacitance is approximately 50 nF, the added inductance L is 100 mH; and thus the optimal switching-on time is half of the period of the LC loop, which is approximately 222 μs. In the LC oscillator, when the voltage of the capacitor has the positive peak voltage, choosing half of the period theoretically can flip the capacitor voltage to the negative peak, which saves the energy dissipated on the harvester capacitance. When the switching-on time is away from half of the period, the harvester voltage can be flipped to a voltage in between. In validation experiments, it can only flip V_T from $V_{rect}+2V_{th}$ to $-V_{invert}$ which is close to $-(V_{rect}+2V_{th})$, when the switching time is 222 μs. From V_{invert} to the negative peak, a charging process can be observed from the measured TEH voltage waveform in the experiment as Fig. 16 (e). With mismatching of half of the period, the SSHI rectifier cannot work. Fig. 19 shows the results of TEH voltage with the different switching-on time of 125 μs, 222 μs, and 444 μs with the input frequency of 4 Hz. When the switching-on time is 125 μs, the flipping can be partially achieved as Fig. 19 (a); when that is 444 μs which is one period, the capacitor voltage in the RLC circuit theoretically

This article has been accepted for publication in a future issue of this journal, but has not been fully edited. Content may change prior to final publication. Citation information: DOI 10.1109/TPEL.2019.2934676, IEEE Transactions on Power Electronics

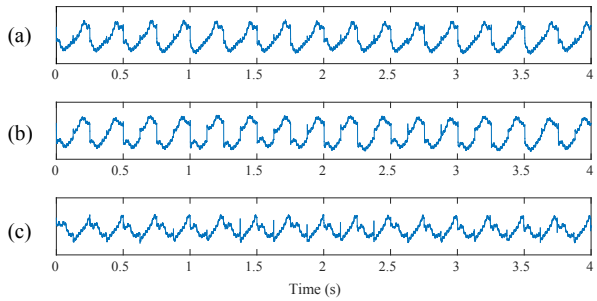

Fig. 19 TEH voltage with an SSHI interface with different switching-on time of (a) 125 μs, (b) 222 μs (c) 444 μs.

goes back to $V_{rect}+2V_{th}$ and will not be flipped. In the experiment, we also cannot observe voltage flipping as Fig. 19 (c).

V. Conclusion

In this paper, an SSHI rectifier for triboelectric energy harvesting is first attempted and reported. A new design of TEH with a multilayer structure is developed with the consideration of the source capacitance. A theoretical model is also developed to understand triboelectric energy harvesting in practical application and guide SSHI design. The experimental results show that the harvested power can be significantly improved by the proposed SSHI rectifier. The enhancement by the proposed synchronized switching approach is up to 242.83% compared to using a bridge rectifier. The introduction of the SSHI interface provides a promising strategy for enhancing power generation of triboelectric energy harvesting in the ac-dc stage.

References

[1] F.R. Fan, Z.Q. Tian, and Z.L. Wang, "Flexible triboelectric generator," *Nano energy*, vol. 1, no. 2, pp. 328-334, 2012.

[2] X. Li, H. Huang, and Y. Sun, "Tribowalk: Triboelectric dual functional wireless system for gait monitoring and energy harvesting," In *2016 IEEE-EMBC'16*, Aug. 2016, pp. 4796-4799.

[3] C. Dagdeviren, Z. Li, and Z.L. Wang, "Energy harvesting from the animal/human body for self-powered electronics", *Annu. Rev. Biomed. Eng.*, vol. 19, pp. 85-108, 2017.

[4] X. Li and Y. Sun, "WearETE: A scalable wearable e-textile triboelectric energy harvesting system for human motion scavenging," *Sensors*, vol. 17, no. 11, pp. 2649, 2017.

[5] F.R. Fan, W. Tang, and Z.L. Wang, "Flexible nanogenerators for energy harvesting and self-powered electronics," *Adv. Mater.*, vol. 28, no. 22, pp. 4283-4305, 2016.

[6] X. Pu, L. Li, H. Song, C. Du, Z. Zhao, C. Jiang, G. Cao, W. Hu, and Z.L. Wang, "A self‐charging power unit by integration of a textile triboelectric nanogenerator and a flexible lithium‐ion battery for wearable electronics," *Adv. Mater.*, vol. 27, no. 15, pp. 2472-2478, 2015.

[7] X. Pu, M. Liu, X. Chen, J. Sun, C. Du, Y. Zhang, J. Zhai, W. Hu, and Z.L. Wang, "Ultrastretchable, transparent triboelectric nanogenerator as electronic skin for biomechanical energy harvesting and tactile sensing," *Sci. adv.*, vol. 3, no. 5, p.e1700015, 2017.

[8] F. Chen, Y. Wu, Z. Ding, X. Xia, S. Li, H. Zheng, C. Diao, G. Yue, Y. Zi. "A novel triboelectric nanogenerator based on electrospun polyvinylidene fluoride nanofibers for effective acoustic energy harvesting and self-powered multifunctional sensing," *Nano energy*. 2018.

[9] H. Ryu, J.H. Lee, U. Khan, S.S. Kwak, R. Hinchet, S.W. Kim. "Sustainable direct current powering a triboelectric nanogenerator via a novel asymmetrical design," *Energy Environ. Sci.*, 2018.

[10] F. Xi, Y. Pang, W. Li, T. Jiang, L. Zhang, T. Guo, G. Liu, C. Zhang, and Z.L. Wang, "Universal power management strategy for triboelectric nanogenerator," *Nano Energy*, vol. 37, pp. 168-176, 2017.

[11] D. Bao, L. Luo, Z. Zhang, and T. Ren, "A power management circuit with 50% efficiency and large load capacity for triboelectric nanogenerator," *J. Semicond.*, vol. 38, no. 9, pp. 095001, 2017.

[12] X. Cheng, L. Miao, Y. Song, Z. Su, H. Chen, X. Chen, J. Zhang, and H. Zhang, "High efficiency power management and charge boosting strategy for a triboelectric nanogenerator," *Nano Energy*, vol. 38, pp. 438-446, 2017.

[13] I. Park, J. Maeng, D. Lim, M. Shim, J. Jeong, and C. Kim, "A 4.5-to-16μW integrated triboelectric energy-harvesting system based on high-voltage dual-input buck converter with MPPT and 70V maximum input voltage," In *2018 IEEE ISSCC*, Feb. 2018, pp. 146-148.

[14] H. Qin, G. Cheng, Y. Zi, G. Gu, B. Zhang, W. Shang, F. Yang, J. Yang, Z. Du, Z.L. Wang, "High energy storage efficiency triboelectric nanogenerators with unidirectional switches and passive power management circuits," *Adv. Funct. Mater.*, pp.1805216, 2018.

[15] P. Vasandani, B. Gattu, Z.H. Mao, W. Jia, M. Sun, "Using a synchronous switch to enhance output performance of triboelectric nanogenerators," *Nano Energy*. vol. 43, pp. 210-8, 2018.

[16] D. Guyomar, A. Badel, E. Lefeuvre, and C. Richard, "Toward energy harvesting using active materials and conversion improvement by nonlinear processing," *IEEE Trans. Ultrason. Eng.*, vol. 52, no. 4, pp.584-595, 2005.

[17] L. Garbuio, M. Lallart, D. Guyomar, C. Richard, and D. Audigier, "Mechanical energy harvester with ultralow threshold rectification based on SSHI nonlinear technique," *IEEE Trans. Ind. Electron.*, vol. 56, no. 4, pp. 1048-1056, 2009.

[18] J. Liang and W.H. Liao, "Improved design and analysis of self-powered synchronized switch interface circuit for piezoelectric energy harvesting systems". *IEEE Trans. Ind. Electron*, vol. 59, no. 4, pp. 1950-1960, 2012.

[19] Alphalab Inc. (2018, Dec.). "The Triboelectric Series," [Online]. Available: http://www.trifield.com/content/tribo-electric-series/.

[20] S. Niu and Z.L. Wang. "Theoretical systems of triboelectric nanogenerators". *Nano Energy*, vol. 14, pp. 161-192, 2015.

[21] S. Niu, X. Wang, F. Yi, Y.S. Zhou, and Z.L. Wang, "A universal self-charging system driven by random biomechanical energy for sustainable operation of mobile electronics," *Nat. Commun.*, vol. 6, pp, 8975, 2015.

[22] K. Dai, X. Wang, S. Niu, F. Yi, Y. Yin, L. Chen, Y. Zhang, and Z. You, "Simulation and structure optimization of triboelectric nanogenerators considering the effects of parasitic capacitance," *Nano Research*, Vol. 10, pp.157-171, 2017.

[23] P. Vasandani, Z.H. Mao, W. Jia, and M. Sun. "Relationship between triboelectric charge and contact force for two triboelectric layers." *J. Electrost.,* vol.90, pp. 147-152, 2017.

[24] S. Niu, S. Wang, L. Lin, Y. Liu, Y.S. Zhou, Y. Hu, and Z.L. Wang. "Theoretical study of contact-mode triboelectric nanogenerators as an effective power source." *Energy Environ. Sci.,* vol. 6, no. 12, pp. 3576-3583, 2013.

[25] H. Huang, X. Li, S. Liu, S. Hu, Y. Sun. "TriboMotion: A self-powered triboelectric motion sensor in wearable internet of things for human activity recognition and energy harvesting," *IEEE Internet of Things J.*, 2018.

[26] J.R. Liang and W.H. Liao, "Piezoelectric energy harvesting and dissipation on structural damping," *J. Intell. Mater. Syst. Struct.*, vol. 20, no. 5, pp. 515-527, 2009.

[27] E. Lefeuvre, A. Badel, C. Richard, L. Petit, D. Guyomar, "A comparison between several vibration-powered piezoelectric generators for standalone systems," *Sens. Actuator A-Phys.*, vol. 126, no. 2, pp.405-16, 2006.

[28] D. Guyomar and M. Lallart, "Recent progress in piezoelectric conversion and energy harvesting using nonlinear electronic interfaces and issues in small scale implementation," *Micromachines*,vol. 2, no. , pp. 274-94, 2011.

[29] I.C. Lien, Y.C. Shu, W.J. Wu, S.M. Shiu, H.C. Lin, "Revisit of series-SSHI with comparisons to other interfacing circuits in piezoelectric energy harvesting," *Smart Mater. Struct.,* vol. 19, no. 12, pp.125009, 2010.

[30] S. Lu and F. Boussaid, "A highly efficient P-SSHI rectifier for piezoelectric energy harvesting," *IEEE Trans.Power Electr.,* vol. 30, no. 10, pp. 5364-9, 2015.

[31] A.M. Eltamaly and K.E. Addoweesh, "A novel self-power SSHI circuit for piezoelectric energy harvester". *IEEE Trans. Power Electron.*, vol. 32, no. 10, pp.7663-7673, 2017.

[32] L. Wu, X.-D. Do, S.-G. Lee, and D.S. Ha. "A self-powered and optimal SSHI circuit integrated with an active rectifier for piezoelectric energy

harvesting." *IEEE Trans. Circuits and Sys. Reg. Papers*, vol. 64, no. 3, pp. 537-549, 2019

[33] M. Dini, A. Romani, M. Filippi, and M. Tartagni, "A nanopower synchronous charge extractor IC for low-voltage piezoelectric energy harvesting with residual charge inversion," *IEEE Trans. Power Electron.*, vol. 31, no. 2, pp. 1263–1274, Feb. 2016.

[34] N. Krihely and S. Ben-Yaakov, "Self-contained resonant rectifier for piezoelectric sources under variable mechanical excitation," *IEEE Trans. Power Electron.*, vol. 26, no. 2, pp. 612–621, Feb. 2011.

[35] S. Lu and F. Boussaid, "A highly efficient P-SSHI rectifier for piezoelectric energy harvesting," *IEEE Trans. Power Electron.*, vol. 30, no. 10, pp. 5364–5369, Oct. 2015.

[36] P. Gasnier, S. Boisseau, G. Despesse, C. Condemine, G. Gouvernet, and J.J. Chaillout, "An autonomous piezoelectric energy harvesting IC based on a synchronous multi-shot technique," *IEEE J. Solid-State Circuits*, vol. 49, no. 7, pp. 1561–1570, Jul. 2014.

[37] T. Hehn, F. Hagedorn, D. Maurath, D. Marinkovic, I. Kuehne, A. Frey, A. and Y. Manoli, "A fully autonomous integrated interface circuit for piezoelectric harvesters," *IEEE J. Solid-State Circuits*, vol. 47, no. 9, pp. 2185–2198, Sep. 2012.

[38] E.E. Aktakka and K. Najafi, "A micro inertial energy harvesting platform with self-supplied power management circuit for autonomous wireless sensor nodes," *IEEE J. Solid-State Circuits*, vol. 49, no. 9, pp. 2017–2029, Sep. 2014.

[39] I. Khemili and L. Romdhane, "Dynamic analysis of a flexible slider–crank mechanism with clearance," *Eur. J. Mech. A-Solid*.vol. 27, no. 5, pp.882-98, 2008.

[40] R.J.M. Vullers, R. van Schaijk, I. Doms, C. van Hoof, R. Mertens, "Micropower energy harvesting," *Solid-State Electron.*, vol. 53, pp. 684-693, 2009.

[41] H.S. Kim, J.-H. Kim, and J. Kim, "A review of piezoelectric energy harvesting based on vibration," *Int. J. Precis. Eng. Manuf.*, vol. 12, no. 6, pp. 1129-1141, 2011.

[42] V. Nguyen, R. Yang. "Effect of humidity and pressure on the triboelectric nanogenerator," *Nano Energy*, vol. 2, no. 5, pp. 604-8, 2013.

[43] Y. Zi, S. Niu, J. Wang, Z. Wen, W. Tang, and Z.L. Wang, " Standards and figure-of-merits for quantifying the performance of triboelectric nanogenerators," *Nature Communications*, Vol. 6, p.8376, 2015.

[44] Y. Zi, J. Wang S. Wang, S. Li, Z. Wen, H. Guo, and Z.L. Wang, "Effective energy storage from a triboelectric nanogenerator," *Nature Communications*, Vol. 7, p.10987, 2016.

[45] K.Y. Lee, J, Chun, J.H. Lee, K.N. Kim, N.R. Kang, J.Y. Kim, M.H. Kim, K.S. Shin, M.K. Gupta, J.M. Baik, and S.W. Kim, "Hydrophobic sponge structure based triboelectric nanogenerator," *Advanced Materials*, Vol. 26, pp.5037-5042, 2014.

[46] Q. Liang, X. Yan, Y. Gu, X. Zhang, M. Liang, S. Lu, X. Zheng, and Y. Zhang, "Highly transparent triboelectric nanogenerator for harvesting water-related energy reinforced by antireflection coating," *Scientific Reports*, Vol. 5, p.9080, 2015.

[47] M.L. Seol, J.H. Woo, D.I. Lee, H. Im, J. Hur, and Y.K. Choi, "Nature‐replicated nano-in-micro structures for triboelectric energy harvesting. Small, Vol. 10, pp.3887-3894, 2014.

Xian Li (S' 16) received the B.S. degree in biomedical engineering from Tianjin University, Tianjin, China, in 2012 and the M.S. degree in biomedical engineering from Chongqing University, Chongqing, China, in 2015.

He is currently pursuing his Ph.D. degree in mechanical engineering at Michigan Technological University (MTU), Houghton, Michigan. His research interest includes smart health via machine learning, internet of things, human health monitoring during driving via wireless sensor network, and energy harvesting.

Mr. Li is a recipient of NSF Student Travel Awards and a student member of IEEE.

Ye Sun (M' 14) received the B.S. degree in Instrumentation Engineering from Tianjin University, China, in 2009 and the Ph.D. degree in Electrical Engineering from Case Western Reserve University, Cleveland, OH, in 2014.

She is currently an assistant professor in the Department of Mechanical Engineering-Engineering Mechanics and an affiliated assistant professor in the Department of Biomedical Engineering at Michigan Technological University, Houghton, MI, where she serves as the Director of the Cyber-Physical Systems Center and an Associate Director of the Institute of Computer and Cybersystems. Her research is an interdisciplinary resort that integrates engineering innovation with human health and human behaviors.

Dr. Sun is a recipient of the NSF CAREER Award and an active member of IEEE and ASME.